Supporting Information

Henzie et al. 10.1073/pnas.1218616110

SI Materials and Methods

Chemicals. Silver nitrate ($AgNO_3$, 99.9999% trace metals basis), PVP (55,000 MW), DMF (>99.9%), and ethanol were purchased from Sigma Aldrich. Tridecafluoro-1,1,2,2-tetrahydrooctyl-1-trichlorosilane was purchased from Gelest, Inc. All chemicals were used without further purification.

Template Fabrication. Templates were fabricated with NIL using a quartz nanoimprinting master. PMMA 100-nm thick was spun on quartz chips of 1" size and subjected to electron beam exposure on a FEI SEM system equipped with Nabbity Lithography System. After the patterns were developed, 10 nm Cr was evaporated on the quartz surface and subsequently lifted off. The substrate was RIE etched to a thickness of around 80 nm onto quartz to serve as nanoimprinting master. Next the quartz master was used to transfer the patterns onto a nanoimprinting resist on Si, and 10 nm of Cr was evaporated on the surface followed by liftoff to generate the pattern. RIE eching produced pits in Si of the desired thickness, followed by metal removal. These templates were sonicated in DI water followed by ethanol and then treated with Tridecafluoro-1,1,2,2-tetrahydrooctyl-1-trichlorosilane, same as the glass coverslips.

Confocal Raman Microspectroscopy. All measurements were performed on a Jobin-Yvon LabRAM HR confocal epi-microscope collecting with 100× (0.9 N.A.) or 20× (0.25 N.A.) objectives. Linearly polarized laser sources were used, so the polarization of the light could be rotated with a half-wave plate, or converted into circularly polarized light with a quarter-wave plate. In a typical measurement, the sample area was defined in the software and given a step size of 0.5 microns between each confocal acquisition point. The laser was focused on the sample and polarized depending on particle assembly orientation. The Raman scattered photons were passed through a circular polarizer before being measured by the spectrometer.

Particles were assembled on the substrate before passivation with 4-AMT. We sparged 50 mL of ethanol with argon for 2 h, and 1 mg of 4-AMT was added to the solution. Then the assembled substrates were placed in solution for ∼12 h, keeping argon bubbling in solution to avoid any oxidation. These samples were then immediately imaged on the confocal Raman microscope. Imaging experiments were performed under both air and argon atmosphere, but there was no noticeable difference in SERS EF, indicating that oxidation happened over a much longer timescale.

Calculation of Single SERS Enhancement. The experimental SERS enhancement was calculated using the 1,078 cm^{-1} of 4-AMT with the SSEF calculation describe by Le Ru et al. (1):

$$SSEF = \frac{I_{SERS}/(\mu_M \mu_s A_M)}{I_{RS}/(c_{RS} H_{eff})},$$

where I_{SERS} is the intensity of the Raman signal in counts per second (cts/s) from the largest single acquisition point corresponding to the location of the particle assembly; μ_M is the surface density of the individual assemblies, which in these experiments is one; μ_S is the surface density of 4-AMT on the Ag surface; A_M is the surface area of the particle assembly; I_{RS} is the intensity of the non-SERS sample; c_{RS} is the concentration of the non-SERS sample; and H_{eff} is the effective height of the scattering volume, which is determined by the thickness of the non-SERS cell. This method assumes a close-packed self-assembled monolayer and averages the SERS enhancement over the entire sample area instead of just the tips, edges, and gaps where the EM field is typically the strongest.

Transmission Electron Microscopy and Characterization of the Interparticle Gap. For the TEM measurements, particles were assembled on 15-nm-thick silicon nitride windows (Ted Pella, Inc.) by drying a solution of particles (∼0.1 μg/μL) on its surface. The spacing between Ag nanocubes in a single dimer was measured by transmission electron microscopy in both an FEI Tecnai F20-UT and FEI Titan 80–300 (equipped with two CEOS hexapole-type spherical aberration correctors), operated at 200 and 300 KV, respectively. Since the gap runs along an atomically smooth face of each nanocube, alignment to the [100] zone axis of a single nanocube in the dimer is sufficient for parallel viewing of the gap. The slight rotational offset about the dimer axis nearly always precludes the existence of both particles being perfectly aligned to the same zone axis. The displacement in the diffraction patterns relative to each other always occurs in the direction parallel to the gap. No shift in diffraction patterns with respect to the other was observed in the perpendicular direction, meaning there exists constant gap width parallel to the electron beam at any given point along the interface. Fig. S1 shows the importance of focus, where underfocus leads to lattice fringes impinging into the vacuum. The interparticle gaps were also measured on SiO windows and amorphous carbon membranes, but we observed no variation in the gap size (Fig. S2).

Nanoparticle Synthesis and Etching

This shape-controlled nanoparticle synthesis has undergone a few modifications since it was developed by the Yang laboratory (2, 3). Briefly, 70 mg of copper(II) chloride was dissolved in 10 mL of 1,5-pentanediol (PD) and sonicated until dissolved. Then 35 μL of this solution was added to a vial containing 10 mL of PD, along with 0.4 g of $AgNO_3$ and sonicated until the color of the solution changed from clear to orange and all $AgNO_3$ was dissolved. In a separate vial, 0.4 g of polyvinylpyrrolidone (PVP) was added to 10 mL of PD, and then sonicated until dissolved.

Next a 100 mL round bottom flask was filled with 20 mL of PD, and heated in a temperature-controlled silicone oil bath until the internal temperature of the PD was 150 °C. As noted by Wiley (4), the reducing power of the diol solvent depends strongly on temperature, which affects the nucleation and growth of the particles. In a typical reaction it takes 4 min to heat the reaction from RT to 150 °C before initiating the synthesis. Once this temperature was achieved, both precursor solutions were added at a rate of 0.5 mL/min for ∼20 min until the cubes were formed. Additional precursor solution of the same concentration can be added at the same rate, forming cubes that progressively truncate to form truncated cubes, cuboctahedra, truncated octahedra, and finally octahedra. Once the octahedra is formed, additional precursor adds to the (111) facet, making increasingly larger octahedra.

The mildly etched octahedra were synthesized by the method describe by Mulvihill et al. (3). Briefly, a solution containing 45 mL concentrated ammonium hydroxide and 5 mL of 30% hydrogen peroxide was prepared and held on ice at 4 °C. We added 100 μL of the etchant to an aqueous solution of PVP (1 mg/mL) under vigorous stirring, followed immediately by 500 μL solution of Ag octahedral particles. After 5 min, the etched particles were centrifuged from solution and resuspended in DMF or ethanol.

Electromagnetic Calculations

For the finite-difference time domain (FDTD) simulations, nanocubes with an edge length (a) of 122 nm and edges and corners with a radius of curvature (r_c) of 10 nm and a gap size of 1.5 nm were meshed at 0.5 nm along all directions. Nanocube dimers were relatively small compared with the octahedra dimers and could be monitored in 3D along all points in the mesh, measuring the local electromagnetic field intensity and the local refractive index to generate the field polarization maps. The calculated octahedral dimers had an edge length of 300 nm and edges and tips with a radius of curvature of 20 nm and a gap of 1.5 nm. Since the octahedra were considerably larger, and could only be meshed at 1 nm along the x–y axis (parallel to the gap) and 0.5 nm along the z axis. Monitoring the electric field intensity and local refractive index of the entire particle was not computationally feasible, so we monitored a $320 \times 320 \times 50$ nm (xyz) box with the interparticle gap and particle dimer in the center. The dielectric function of the silver polyhedra was taken from the bulk silver measurement described by Palik (5).

1. Rue ECL, et al. (2007) Surface enhanced raman scattering enhancement factors: A comprehensive study. *J Phys Chem B* 111(37):13794–13803.
2. Tao A, et al. (2008) Shape control of colloidal metal nanocrystals. *Small* 4(3):310–325.
3. Mulvihill MJ, Ling XY, Henzie J, Yang P (2010) Anisotropic etching of silver nanoparticles for plasmonic structures capable of single-particle SERS. *J Am Chem Soc* 132(1):268–274.
4. Wiley B, Sun Y, Mayers B, Xia Y (2005) Shape-controlled synthesis of metal nanostructures: the case of silver. *Chemistry* 11(2):454–463.
5. Palik E (1998) *Handbook of Optical Constants of Solids* (Academic, New York), Vol. 1–3.

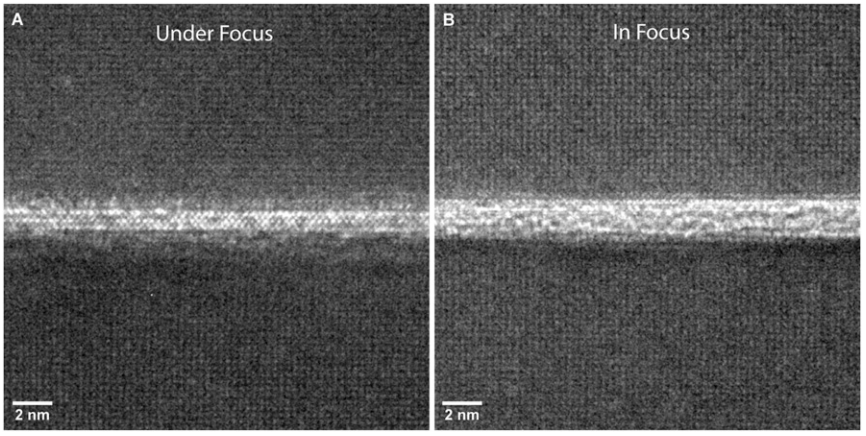

Fig. S1. Bright-field transmission electron microscopy (TEM) images of an interparticle gap that is underfocused (*A*) and in focus (*B*). When the image is underfocused, lattice fringes impinge on the interparticle gap and obscure its true dimensions.

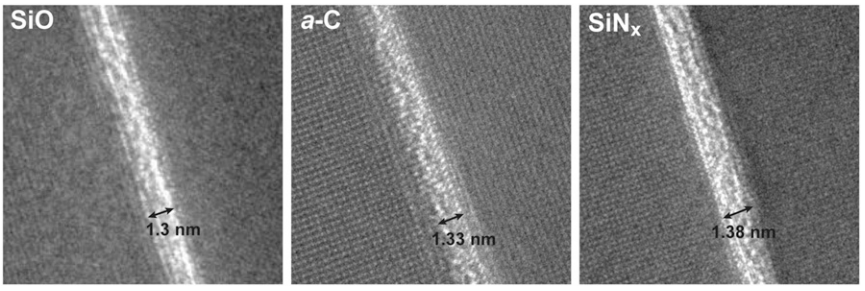

Fig. S2. TEM measurements from SiNx, SiO, and amorphous carbon films. These substrates vary in surface energy, but we saw no variation in gap size outside of the SD.

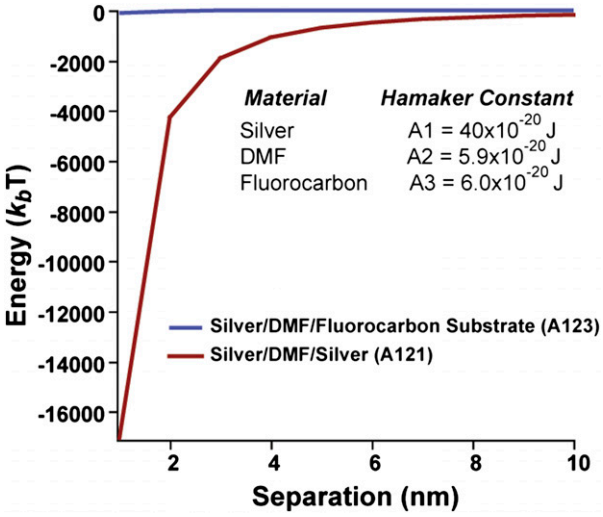

Fig. S3. A comparison of the calculated van der Waals (vdW) forces between two adjacent Ag octahedra in DMF, and the force between an Ag octahedron and the fluorocarbon substrate. Each octahedra has an edge length of 300 nm. The vdW forces between the metal surface are very strong at small separations. (The formulas and Hamaker constants used to calculate vdW forces can be found in ref. 1. The value of the Hamacker constant for a fluorocarbon surface was found in ref. 2.)

1. Israelachvili J (1991) *Intermolecular and Surface Forces* (Academic, New York), 2nd Ed., pp 200–206.
2. Takenaga M, Jo S, Graupe M, Lee TR (2008) Effective van der Waals surface energy of self-assembled monolayer films having systematically varying degrees of molecular fluorination. *J Colloid Interface Sci* 320(1):264–267.

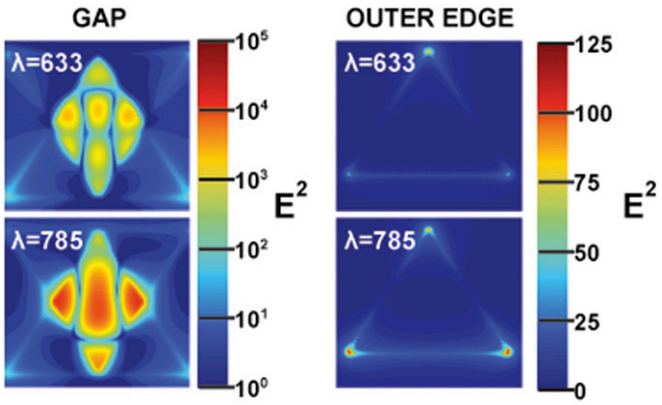

Fig. S4. The EM intensity of the face-to-face octahedral dimer at the gap (*Left*) compared with the outer edge facet (*Right*) at the surface-enhanced Raman spectroscopy laser excitation wavelengths. The intensity inside the gap is many orders of magnitude larger.

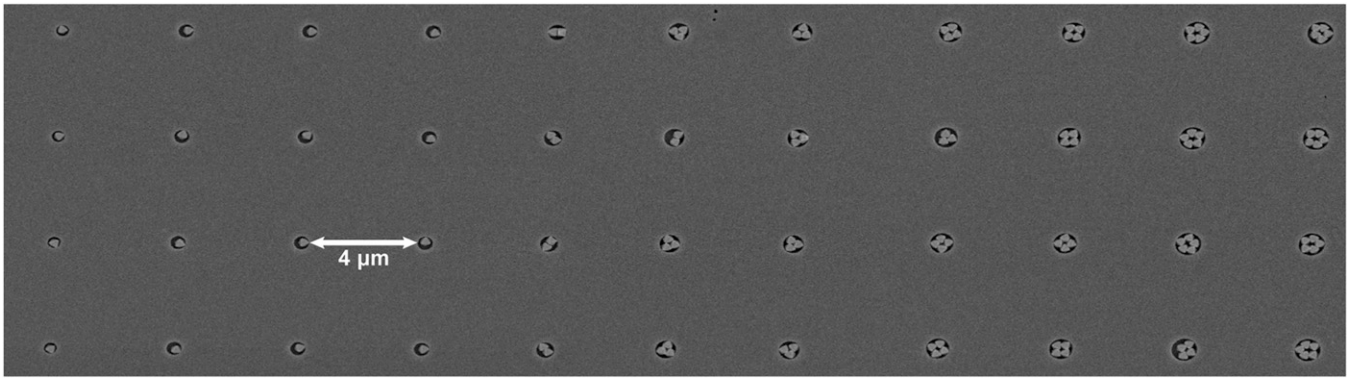

Fig. S5. Octahedra assembled into circular pits with a depth of 300 nm and diameters of 450–950 nm at 50-nm step intervals.

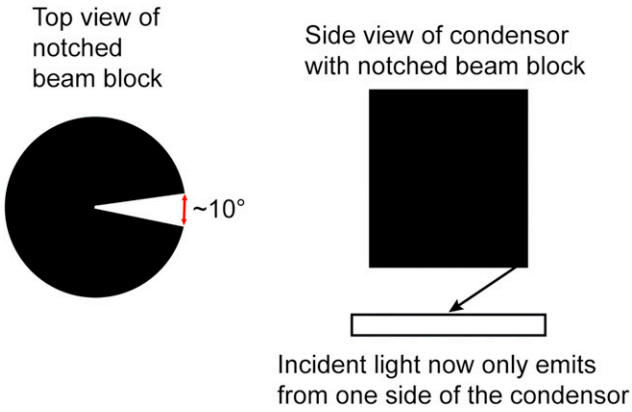

Fig. S6. Illustration of the beam block used to ensure that only light from one side of the condensor was illuminating the particles.

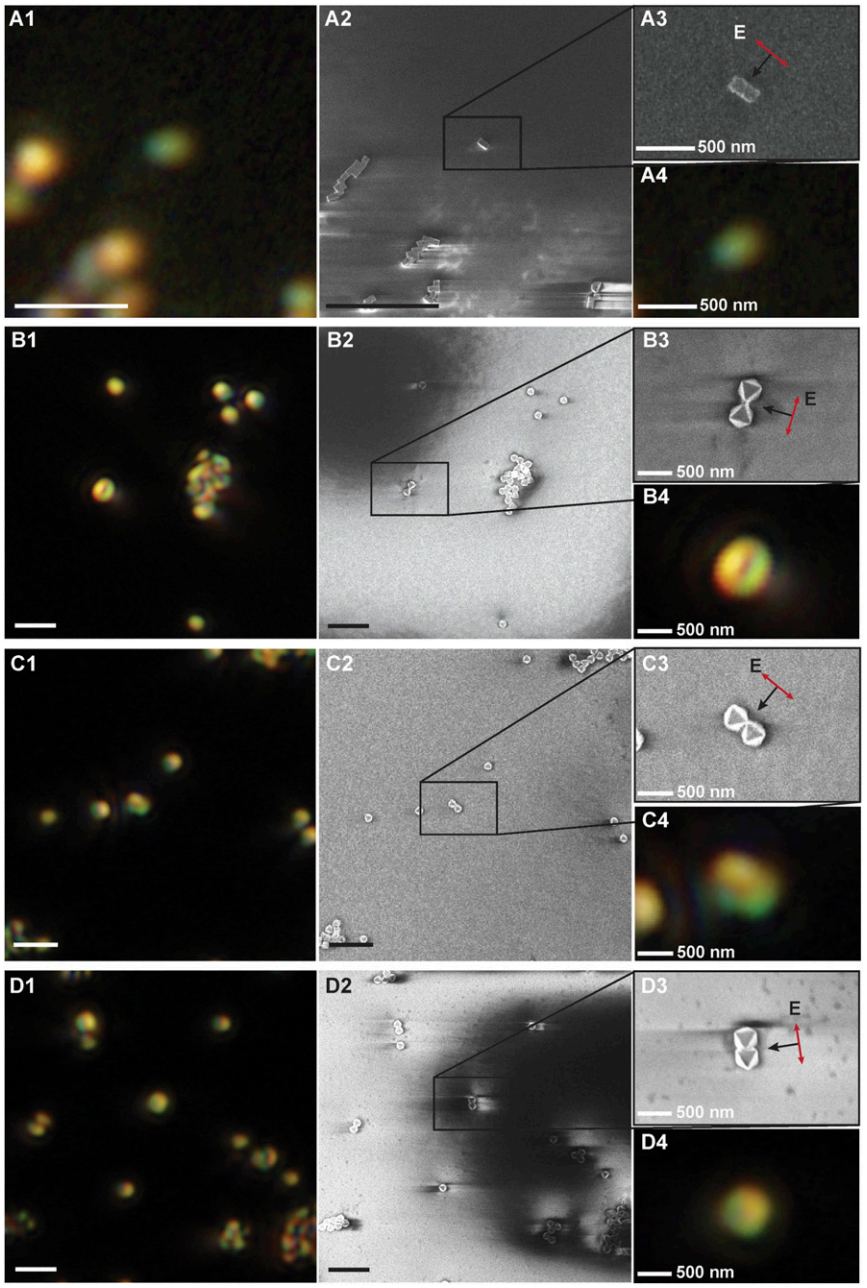

Fig. S7. Optical micrographs show particle dimers (*A1*, *B1*, *C1*, and *D1*) that were measured using dark field microspectroscopy. Afterward, these samples were imaged using SEM to determine their precise orientation (*A2*, *B2*, *C2*, and *D2*). Zoom-in images indicate the rough orientation of the particles can be determined optically (*A3–4*, *B3–4*, *C3–4*, and *D3–4*). All scale bars are 2 μm unless otherwise noted.

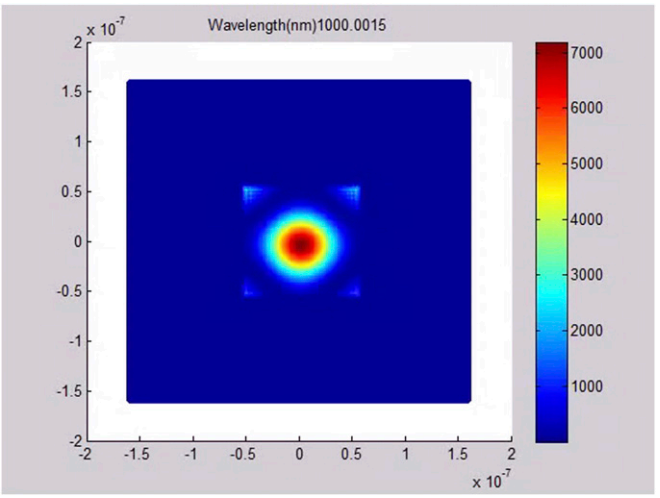

Movie S1. Electromagnetic intensity versus wavelength within the center of the interparticle gap for dimers of nanocubes.

Movie S1

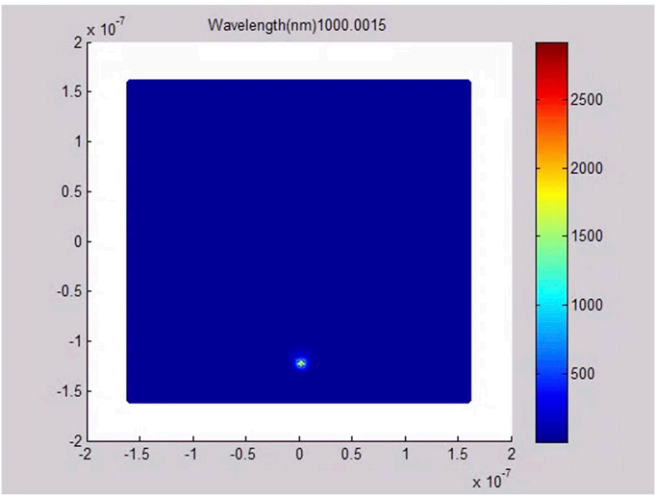

Movie S2. Electromagnetic intensity versus wavelength within the center of the interparticle gap for dimers of tip-to-tip octahedra.

Movie S2

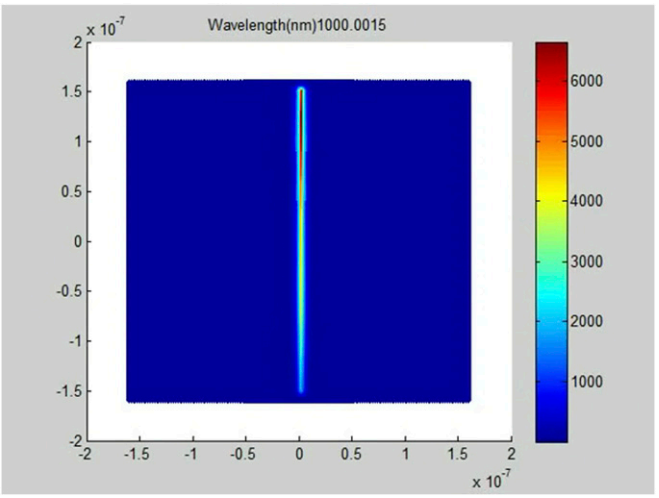

Movie S3. Electromagnetic intensity versus wavelength within the center of the interparticle gap for dimers of edge-to-edge octahedra.

Movie S3

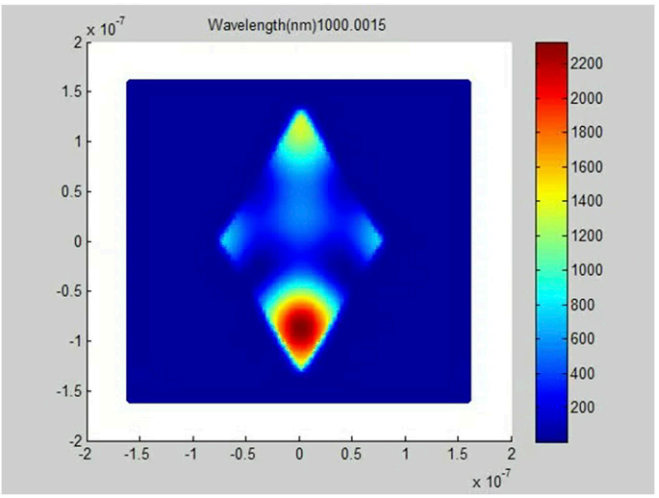

Movie S4. Electromagnetic intensity versus wavelength within the center of the interparticle gap for dimers of face-to-face octahedra.

Movie S4